

High Impedance Josephson Junction Resonators in the Transmission Line Geometry

Antti Ranni,^{a)} Harald Havar, Subhomoy Haldar, and Ville F. Maisi^{b)}

NanoLund and Solid State Physics, Lund University, Box 118, 22100 Lund, Sweden

(Dated: 23 June 2023)

In this article we present an experimental study of microwave resonators made out of Josephson junctions. The junctions are embedded in a transmission line geometry so that they increase the inductance per length for the line. By comparing two devices with different input/output coupling strengths, we show that the coupling capacitors, however, add a significant amount to the total capacitance of the resonator. This makes the resonators with high coupling capacitance to act rather as lumped element resonators with inductance from the junctions and capacitance from the end sections. Based on a circuit analysis, we also show that the input and output couplings of the resonator are limited to a maximum value of $\omega_r Z_0 / 4Z_r$ where ω_r is the resonance frequency and Z_0 and Z_r are the characteristic impedances of the input/output lines and the resonator respectively.

High impedance resonators have obtained a significant attention in recent years. They have been used to obtain strong coherent coupling of microwave photons to semiconducting charge¹ and spin²⁻⁵ qubits. In addition, the high impedance materials⁶⁻¹² and superconductors¹³⁻¹⁵ are highly useful for realizing e.g. amplifiers^{16,17} and qubits¹⁸⁻²⁰. The increased coupling of the added inductance gives rise to accessing the so-called ultra-strong coupling regime^{21,22}, which is predicted to give rise to new fundamental physics concepts such as electroluminescence from the ground state²³. In this letter, we investigate high impedance ($Z_r \sim 1\text{k}\Omega$) resonators in a plain transmission line geometry made out of Josephson junctions. We show that by using such a definite geometry allows us to determine unambiguously the internal losses of the resonator, as well as to show how the input coupling influences on the resonator properties: a modest increase of the input coupling from $\kappa_c/2\pi = 3.5\text{ MHz}$ to 11 MHz leads to a 20% reduction of the resonance frequency and the characteristic impedance. Based on these findings, we determine that - despite the ultra-strong coupling to quantum structures up to 0.6 GHz coupling is achievable²² - the input coupling is limited to $\kappa_c = \omega_r Z_0 / 4Z_r$ where Z_0 is the characteristic impedance of the input lines and ω_r the resonance frequency. For our resonators, representing typical parameter values in the recently realized experiments^{1,8,22}, the largest possible coupling is limited to $\kappa_c/2\pi = 90\text{ MHz}$. This imposes a trade-off between the input line coupling and the electric-dipole coupling to a quantum device. The results are important for designing and optimizing the high impedance resonator devices.

Figure 1 (a) shows the studied resonator. A Josephson junction chain defines a high impedance transmission line geometry^{7,8,13,14,16} where each Josephson junction yields an inductance $L_J = hR_T/2\pi^2\Delta$. Here $R_T = 500\Omega$ is the normal state resistance of the junction, measured from similar junctions fabricated at the same processing round as the resonator, and $\Delta = 200\mu\text{eV}$ the superconducting gap of aluminum used as the superconductor. The junction separation of $s = 1\mu\text{m}$ yields

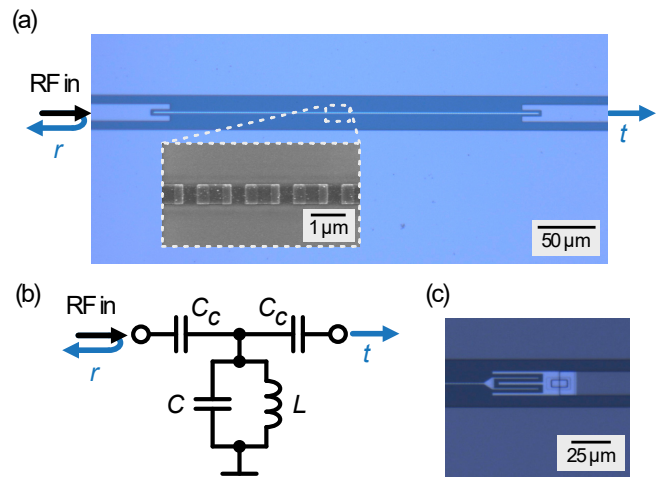


FIG. 1. (a), Optical microscope image of the studied resonator with low input/output coupling strength. The thin line in the middle consists of Al-AlOx-Al Josephson junction chain forming the resonator on top of a silicon substrate with a 200 nm thick oxide layer. Thicker input and output lines to the left and right, together with the ground planes on top and bottom are made of Nb. An RF signal is sent in from the left port and the reflected signal with amplitude r and transmission to the right port with amplitude t are measured. The inset shows the Josephson junctions that form the high impedance resonator in between. (b), The electrical circuit equivalent to the resonator. The fundamental resonance mode corresponds to an LC resonator with the capacitance C and inductance L . The capacitances C_c set the input couplings. (c), Optical microscope image of the coupler geometry for the high input/output coupling resonator.

the inductance per unit length of $l = L_J/s = 500\mu\text{H/m}$. This value is more than two orders of magnitude larger than the the permeability of vacuum μ_0 which sets the typical value for non-magnetic materials. The high inductance slows down the speed of the signal¹⁶ such that our transmission line with the total length of $d = 231\mu\text{m}$ forms a $\lambda/2$ -resonance mode in the $4 - 8\text{ GHz}$ frequency band. This resonance mode corresponds to an equivalent LC-circuit of Fig. 1 (b) with inductance $L = 2l d/\pi^2$ and capacitance $C = c d/2$ where c is the capacitance per length²⁴.

To probe the resonator properties, we couple the resonator

^{a)}Electronic mail: antti.ranni@ftf.lth.se

^{b)}Electronic mail: ville.maisi@ftf.lth.se

to standard $Z_0 = 50\Omega$ input and output lines with coupling capacitors C_c that are identical for the input and output. Figure 2 (a) presents the measured transmission $|t|^2$ and reflection $|r|^2$ coefficient as a function of the drive frequency ω . A Lorentzian resonance mode at a resonance frequency of $\omega_r/2\pi = 8.735$ GHz is seen in the resonator response. The solid lines show fits to

$$\begin{cases} |t|^2 = \frac{\kappa_c^2}{(\kappa_c + \kappa_i/2)^2 + (\omega - \omega_r)^2} \\ |r|^2 = \frac{(\kappa_i/2)^2 + (\omega - \omega_r)^2}{(\kappa_c + \kappa_i/2)^2 + (\omega - \omega_r)^2}, \end{cases} \quad (1)$$

where $\kappa_i/2\pi = 1.2$ MHz is the internal losses of the resonator and $\kappa_c/2\pi = 3.5$ MHz the input coupling²⁵. The input coupling and the resonator frequency are connected to the circuit elements of Fig. 1 (b) as $\kappa_c = \omega_r^2 C_c^2 Z_0 / C_\Sigma$ and $\omega_r = 1/\sqrt{LC_\Sigma}$ with the total capacitance $C_\Sigma = C + 2C_c$ of the resonator^{24,25}.

In the fits of Fig. 2 (a), the two input couplings $2\kappa_c$ set essentially the linewidth of the resonance and the internal losses κ_i how high the transmission coefficient $|t|^2$ increases and reflection coefficient $|r|^2$ decreases in resonance. The resonator reaches close to the ideal values $|r| = 0$ and $|t| = 1$ of a lossless resonator, reflecting the fact that the internal losses κ_i are significantly smaller than the couplings κ_c . With the Josephson junction parameter values and the fits above, we obtain $C_\Sigma = 14$ fF and $C_c = 1.4$ fF. The characteristic impedance of the resonator is then $Z_r = \sqrt{L/C_\Sigma} = 1.4\text{k}\Omega$. Note that here we use the characteristic impedance of the full circuit at the end points of the resonator. Hence this value describes the effective impedance value to which other circuit elements couple when connecting them to the typical maximal coupling point at the end of the resonator with a voltage antinode. The characteristic impedance of the Josephson junction array, $Z_{JJ} = \sqrt{I/c} = 2.4\text{k}\Omega$, is close to this value but naturally doesn't depend on the coupling capacitance C_c like Z_r does. The capacitance per unit length of the junction array $c = 2C/d = 80$ pF/m matches well with similar transmission line geometries on a silicon substrate²⁴.

Next, we consider a resonator with larger input and output couplings. The Josephson junction chain of the resonator is kept the same and was fabricated in the same processing round as the low coupling device of Fig. 1 (a). The input and output couplings are made larger by using an inter-digitized finger geometry shown in Fig. 1 (c). The resulting response is presented in Fig. 2 (b) together with the fits yielding $\omega_r/2\pi = 6.773$ GHz, $\kappa_c/2\pi = 11$ MHz and $\kappa_i/2\pi = 1.3$ MHz. With the same inductance L from the Josephson junction chain, the corresponding circuit parameter values are thus $C_\Sigma = 23$ fF and $C_c = 4.1$ fF resulting in $Z_r = \sqrt{L/C_\Sigma} = 1.0\text{k}\Omega$.

When comparing the two resonator responses, we see that despite the input/output coupling is increased merely to $\kappa_c/2\pi = 11$ MHz, the resonance frequency drops by 2 GHz. This shift arises as the coupling capacitances $2C_c$ contribute to nearly half of the total capacitance C_Σ for the high coupling resonator. Correspondingly, the characteristic impedance Z_r drops by the equal amount of 20% due to the significant added capacitance. On the other hand, the nearly unaltered internal losses κ_i and the Josephson junction chain capacitance of

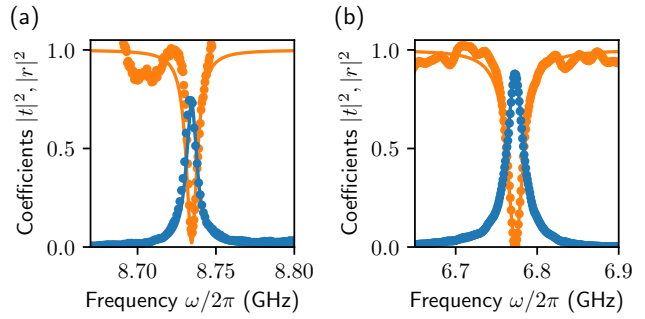


FIG. 2. (a), The measured transmission $|t|^2$ (solid blue dots) and reflection $|r|^2$ (solid orange dots) coefficients as a function of the drive frequency ω . The solid lines show corresponding fits to Eq. (1) with resonance frequency $\omega_r/2\pi = 8.735$ GHz, input/output coupling $\kappa_c/2\pi = 3.5$ MHz and internal losses $\kappa_i/2\pi = 1.2$ MHz. (b), The same measurements repeated for the high input/output coupling resonator. The fit parameter values are $\omega_r/2\pi = 6.773$ GHz, $\kappa_c/2\pi = 11$ MHz and $\kappa_i/2\pi = 1.3$ MHz. The measurements are done at the base temperature of 10 mK in a dilution refrigerator and the drive power applied to the left port is -115 dBm.

$C = 11$ fF for the low coupling resonator versus $C = 15$ fF for the high coupling resonator yield good consistency checks for our model. The extra capacitance of 4 fF in the high coupler resonator is likely due to the increased self capacitance and extra capacitance to ground from the inter-digitized couplers. Indeed, the extra length of $\Delta l = 40\mu\text{m}$ from the couplers corresponds to a capacitance of $c \Delta l = 3$ fF.

The above comparison of the two resonators yields two important points for high impedance resonator designing: 1) Even with the rather small input couplings, one needs to pay extra attention to the added total capacitance that may otherwise shift the resonance frequency uncontrollably far away from the desired value, as well as lower the resonator impedance Z_r . This is in stark contrast to the low impedance 50Ω resonators where the resonance frequency shift is comparable to the coupling κ_c , see e.g. Ref. 24. 2) The significant contribution of the coupling capacitances to the total capacitance limits the highest attainable input/output coupling value $\kappa_{c,\text{max}}$. We obtain this largest coupling by taking the coupling capacitance to dominate the total capacitance, i.e. $C_c \gg C$, which yields $C_\Sigma = 2C_c$ and the highest coupling as

$$\kappa_{c,\text{max}} = \frac{\omega_r^2 C_c^2 Z_0}{C_\Sigma} = \frac{\omega_r^2 C_\Sigma Z_0}{4} = \frac{Z_0}{4Z_r} \omega_r. \quad (2)$$

In the last equality, we used the relation $\omega_r Z_r = 1/C_\Sigma$. For our resonators, exemplary for typical ones used in the experiments, we have $\kappa_{c,\text{max}}/2\pi = 90$ MHz with $Z_r = 1\text{k}\Omega$ and $\omega_r/2\pi = 7$ GHz. Interestingly, these kind of resonators have been shown to yield coherent coupling in the strong and ultra-strong coupling regime for interactions between the microwave photons in the resonator and a charge degree of freedom in a semiconducting quantum dots²². In these experiments, the dipole coupling value reached up to $g/2\pi = 600$ MHz. However, in terms of the resonator input coupling, the system is limited to values much smaller than this.

To recover the low impedance result connecting the frequency shift to the input coupling directly, the same characteristic impedance could be used for both the resonator and the input and output lines with $Z_0 = Z_r$. Forming the input and output lines with the Josephson junction arrays approach would be possible for our resonators without any further processing steps. However, an additional consideration would be needed for connecting the lines further to the usually used standard 50Ω cabling. A "tapering" of the characteristic impedance by increasing the junction separation s gradually along the line could be used. The high kinetic inductance approaches^{6,9,10,12} would offer also a viable option here as the characteristic impedance could be changed by widening the input and output lines gradually with the tapering.

In conclusion, we have measured the transmission and reflection coefficient response of high impedance transmission line resonators made out of Josephson junctions. By varying the capacitive input coupling, we showed that the capacitance added by the couplers has a much stronger effect on the high impedance resonators in comparison to the low impedance ones. The capacitance both reduces the resonance frequency significantly as well as reduces the impedance level. We also showed that the maximum input/output coupling is reduced and limited to $\kappa_{c,\max} = \omega_r Z_0 / 4Z_r$, despite the dipole coupling is increased to an order of magnitude larger values for the typical resonator impedances values of the order of $Z_r \sim 1\text{k}\Omega$ used in these experiments.

We thank A. Baumgartner, A. Pally, P. Scarlino, C. Schönenberger, C. Thelander and J. Ungerer for fruitful discussions, and Swedish Research Council (Dnr 2019-04111), the Foundational Questions Institute, a donor advised fund of Silicon Valley Community Foundation (grant number FQXi-IAF19-07) and NanoLund for financial support.

- ¹A. Stockklauser, P. Scarlino, J. V. Koski, S. Gasparinetti, C. K. Andersen, C. Reichl, W. Wegscheider, T. Ihn, K. Ensslin, and A. Wallraff, "Strong coupling cavity qed with gate-defined double quantum dots enabled by a high impedance resonator," *Phys. Rev. X* **7**, 011030 (2017).
- ²A. J. Landig, J. V. Koski, P. Scarlino, U. C. Mendes, A. Blais, C. Reichl, W. Wegscheider, A. Wallraff, K. Ensslin, and T. Ihn, "Coherent spin-photon coupling using a resonant exchange qubit," *Nature* **560**, 179–184 (2018).
- ³X. Mi, M. Benito, S. Putz, D. M. Zajac, J. M. Taylor, G. Burkard, and J. R. Petta, "A coherent spin-photon interface in silicon," *Nature* **555**, 599–603 (2018).
- ⁴N. Samkharadze, G. Zheng, N. Kalhor, D. Brousse, A. Sammak, U. C. Mendes, A. Blais, G. Scappucci, and L. M. K. Vandersypen, "Strong spin-photon coupling in silicon," *Science* **359**, 1123–1127 (2018).
- ⁵J. H. Ungerer, A. Pally, A. Kononov, S. Lehmann, J. Ridderbos, C. Thelander, K. A. Dick, V. F. Maisi, P. Scarlino, A. Baumgartner, and C. Schönenberger, "Strong coupling between a microwave photon and a singlet-triplet qubit," *arXiv:2303.16825* (2023), <https://doi.org/10.48550/arXiv.2303.16825>.
- ⁶R. Barends, H. L. Hortensius, T. Zijlstra, J. J. A. Baselmans, S. J. C. Yates, J. R. Gao, and T. M. Klapwijk, "Contribution of dielectrics to frequency and noise of NbTiN superconducting resonators," *Appl. Phys. Lett.* **92** (2008), 10.1063/1.2937837.

- ⁷C. Hutter, E. A. Tholén, K. Stannigel, J. Lidmar, and D. B. Haviland, "Josephson junction transmission lines as tunable artificial crystals," *Phys. Rev. B* **83**, 014511 (2011).
- ⁸N. A. Masluk, I. M. Pop, A. Kamal, Z. K. Minev, and M. H. Devoret, "Microwave characterization of Josephson junction arrays: Implementing a low loss superinductance," *Phys. Rev. Lett.* **109**, 137002 (2012).
- ⁹N. Samkharadze, A. Bruno, P. Scarlino, G. Zheng, D. P. DiVincenzo, L. DiCarlo, and L. M. K. Vandersypen, "High-kinetic-inductance superconducting nanowire resonators for circuit QED in a magnetic field," *Phys. Rev. Appl.* **5**, 044004 (2016).
- ¹⁰N. Maleeva, L. Grünhaupt, T. Klein, F. Levy-Bertrand, O. Dupre, M. Calvo, F. Valenti, P. Winkel, F. Friedrich, W. Wernsdorfer, A. V. Ustinov, H. Rotzinger, A. Monfardini, M. V. Fistul, and I. M. Pop, "Circuit quantum electrodynamics of granular aluminum resonators," *Nature Comm.* **9**, 3889 (2018).
- ¹¹L. Grünhaupt, M. Spiecker, D. Gusekova, N. Maleeva, S. T. Skacel, I. Takmakov, F. Valenti, P. Winkel, H. Rotzinger, W. Wernsdorfer, A. V. Ustinov, and I. M. Pop, "Granular aluminium as a superconducting material for high-impedance quantum circuits," *Nature Materials* **18**, 816–819 (2019).
- ¹²D. Nipce, J. Burnett, and J. Bylander, "High kinetic inductance NbN nanowire superinductors," *Phys. Rev. Appl.* **11**, 044014 (2019).
- ¹³M. T. Bell, I. A. Sadovskyy, L. B. Ioffe, A. Y. Kitaev, and M. E. Gershenson, "Quantum superinductor with tunable nonlinearity," *Phys. Rev. Lett.* **109**, 137003 (2012).
- ¹⁴C. Altimiras, O. Parlavecchio, P. Joyez, D. Vion, P. Roche, D. Esteve, and F. Portier, "Dynamical Coulomb blockade of shot noise," *Phys. Rev. Lett.* **112**, 236803 (2014).
- ¹⁵M. Peruzzo, A. Trioni, F. Hassani, M. Zemlicka, and J. M. Fink, "Surpassing the resistance quantum with a geometric superinductor," *Phys. Rev. Appl.* **14**, 044055 (2020).
- ¹⁶M. A. Castellanos-Beltran and K. W. Lehnert, "Widely tunable parametric amplifier based on a superconducting quantum interference device array resonator," *Appl. Phys. Lett.* **91** (2007), 10.1063/1.2773988.
- ¹⁷C. Macklin, K. O'Brien, D. Hover, M. E. Schwartz, V. Bolkhovsky, X. Zhang, W. D. Oliver, and I. Siddiqi, "A near quantum-limited Josephson traveling-wave parametric amplifier," *Science* **350**, 307–310 (2015).
- ¹⁸V. E. Manucharyan, J. Koch, L. I. Glazman, and M. H. Devoret, "Fluxonium: Single Cooper-pair circuit free of charge offsets," *Science* **326**, 113–116 (2009).
- ¹⁹T. M. Hazard, A. Gynis, A. Di Paolo, A. T. Asfaw, S. A. Lyon, A. Blais, and A. A. Houck, "Nanowire superinductance fluxonium qubit," *Phys. Rev. Lett.* **122**, 010504 (2019).
- ²⁰I. V. Pechenezhskiy, R. A. Mencia, L. B. Nguyen, Y.-H. Lin, and V. E. Manucharyan, "The superconducting quasicharge qubit," *Nature* **585**, 368–371 (2020).
- ²¹A. Frisk Kockum, A. Miranowicz, S. De Liberato, S. Savasta, and F. Nori, "Ultrastrong coupling between light and matter," *Nature Rev. Phys.* **1**, 19–40 (2019).
- ²²P. Scarlino, J. H. Ungerer, D. J. van Woerkom, M. Mancini, P. Stano, C. Müller, A. J. Landig, J. V. Koski, C. Reichl, W. Wegscheider, T. Ihn, K. Ensslin, and A. Wallraff, "In situ tuning of the electric-dipole strength of a double-dot charge qubit: Charge-noise protection and ultrastrong coupling," *Phys. Rev. X* **12**, 031004 (2022).
- ²³M. Cirio, S. De Liberato, N. Lambert, and F. Nori, "Ground state electroluminescence," *Phys. Rev. Lett.* **116**, 113601 (2016).
- ²⁴M. Göppl, A. Fragner, M. Baur, R. Bianchetti, S. Filipp, J. M. Fink, P. J. Leek, G. Puebla, L. Steffen, and A. Wallraff, "Coplanar waveguide resonators for circuit quantum electrodynamics," *J. Appl. Phys.* **104**, 113904 (2008).
- ²⁵H. Hahir, S. Haldar, K. W., S. Lehmann, K. A. Dick, C. Thelander, P. Samuelsson, and V. F. Maisi, "Quantum dot source-drain transport response at microwave frequencies," *arXiv:2303.13048* (2023), <https://doi.org/10.48550/arXiv.2303.13048>.